VI. MICROWAVE ELECTRONICS*

Prof. L. D. Smullin
Prof. H. A. Haus
Prof. S. Saito (Visiting Fellow)

A. Bers
R. M. Bevensee
H. W. Fock†
C. Fried

B. A. Highstrete
A. J. Lichtenberg
A. H. Czarapata

A. THEORY OF MODE COUPLING: A SUMMARY

Studies reported in the last Quarterly Progress Report (1) have been modified and extended. The purpose of these studies is to find a formal basis and justification for Pierce's coupling-of-modes formalism (2) as it applies to uniform slow-wave structures containing two or more subsystems that individually propagate slow waves (e.g., traveling-wave tubes).

If it can be assumed that the coupling is weak, approximations that lead to simple coupling equations like those discussed by Pierce can be made. Specific expressions have been found for the coupling coefficients – for example, for Pierce's K for a traveling-wave tube with a thick beam, which was given in reference 1. We found that the expressions previously derived (1) are not valid at strong coupling; therefore second-order terms must be considered in the coupling coefficients. Expressions that are valid at strong coupling can be obtained if a different approach is taken.

As before, we recognize that the coupling-of-modes formalism discussed by Pierce is, in principle, an expansion of the actual fields in terms of the modes of two (or more) (sub)systems. In the neighborhood of a particular (sub)system, the field expansion in terms of the modes of that particular (sub)system is used to represent the actual field. Expressions were obtained that differ at strong coupling from those given in reference 1.

The method for obtaining them was discussed at the URSI May 1957 meeting in Washington, D.C. A paper on this subject is in preparation.

H. A. Haus

References

1. Quarterly Progress Report, Research Laboratory of Electronics, M.I.T., April 15, 1957, pp. 40-44.
2. J. R. Pierce, Coupling of modes of propagation, J. Appl. Phys. 25, 179-183 (1954).

* This research was supported in part by Purchase Order DDL-B187 with Lincoln Laboratory, which is supported by the Department of the Army, the Department of the Navy, and the Department of the Air Force under Contract AF19(122)-458 with M.I.T.

† From Raytheon Manufacturing Company.

B. CAVITY-TO-HELIX COUPLING

An analysis of the coupling of electromagnetic power from a cavity resonator to a helix that passes through the cavity gap, which was illustrated in the Quarterly Progress Report of January 15, 1957, page 36 (Fig. VI-1), has been completed. The analyzed system, which consists of a sheath helix of radius b surrounded by a conducting cylinder of radius a, is considered to be lossless, to contain a single medium, and to be of infinite length. The procedure consists of expanding the fields of the combined system as a summation of the natural modes of the shielded sheath-helix system, with the cavity gap replaced by a sheet of magnetic current that is placed just inside the outer cylinder and is of a proper configuration for providing the assumed electric-field distribution across the gap at r = a. The current sheet is divided into rings of infinitesimal length to which the transverse fields are matched, the amplitude of a single mode being obtained through the use of the orthogonality conditions for the general uniform cylindrical system given by Kino (1). By superimposing the current-ring solutions and calculating the total power P_h in a single mode ($P_h/2$ in each direction), an expression for a "helix admittance," $G_h = 2P_h/|V|^2$ (where V is the peak gap voltage), is obtained.

$$G_h = \pi^2 a^2 [f(\gamma\ell)]^2 \frac{|H_\theta(a)|^2}{P}$$

where ℓ is the gap length; γ is the transverse propagation constant of the mode; and $H_\theta(a)$ and P are properties of a normalized traveling wave of the mode, being the angular component of the transverse magnetic field evaluated at r = a, and the power associated with the wave. The form of the function, $f(\gamma\ell)$, depends on the electric-field distribution assumed at the gap edge and might be either $\sin\frac{\beta\ell}{2}/\frac{\beta\ell}{2}$ or $J_o\left(\frac{\beta\ell}{2}\right)$, as shown in the Quarterly Progress Report of January 15, 1957, page 36, and further discussed by Beck (2).

By considering the explicit expressions given by Mathers and Kino (3), for the usual slow helix mode, that is, the mode with no angular variation, we obtain

$$G_h = \omega^2 \epsilon^2 \pi^2 a^2 [f(\gamma\ell)]^2 \left(\frac{\gamma}{k}\right)\left(\frac{\gamma}{\beta}\right) I_o^2(\gamma b) \frac{G_{10}^2(\gamma a, \gamma a)}{G_{00}^2(\gamma b, \gamma a)} F^3(\gamma b)$$

$$G_{10}(x, y) = I_1(x) K_o(y) + K_1(x) I_o(y)$$

$$G_{00}(x, y) = I_o(x) K_o(y) - K_o(x) I_o(y)$$

where β is the longitudinal propagation constant ($\beta^2 = \gamma^2 + k^2$), and $F(\gamma b)$, which is plotted by Mathers and Kino (3), is related to the helix impedance by

$$Z = \frac{E_z^2(0)}{\beta^2 P} = \left(\frac{\beta}{k}\right)\left(\frac{\gamma}{\beta}\right)^4 F^3(\gamma b)$$

The Bessel-function combinations, G_{10} and G_{00}, have been tabulated (1). Stark (4) predicts that, for a sufficiently small outer cylinder radius, the tape-helix mode whose fundamental space harmonic corresponds to this sheath-helix mode, is the only mode capable of propagation.

If a cavity with shunt conductance G_s, defined at the gap, is tuned to resonance with the helix inserted, the ratio of cavity-input power to helix-coupled power will be given by

$$\frac{P_h}{P_{in}} = \frac{G_h}{G_s + G_h}$$

B. A. Highstrete

References

1. G. S. Kino, Normal mode theory in perturbed transmission systems, Technical Report 84, Electronics Research Laboratory, Stanford University, May 1955.
2. A. H. W. Beck, Velocity-Modulated Thermionic Tubes (Macmillan Company, New York, 1948), p. 62.
3. G. W. C. Mathers and G. S. Kino, Some properties of a sheath helix with a center conductor or external shield, Technical Report 65, Electronics Research Laboratory, Stanford University, June 1953.
4. L. Stark, Lower modes of concentric line having a helical inner conductor, Technical Report 26, Lincoln Laboratory, M.I.T., July 1953.

C. CURRENT GROWTH IN MULTICAVITY KLYSTRONS*

The propagation of small signals along a drifting electron beam can be described by a set of differential equations, similar to transmission-line equations, which relate the kinetic voltage V and the current modulation I in the beam (1, 2).

$$\frac{dV}{d\theta} = j Z_o I \qquad (1)$$

$$\frac{dI}{d\theta} = j Y_o V \qquad (2)$$

* This work was supported in part by the Office of Naval Research under Contract Nonr 1841(05).

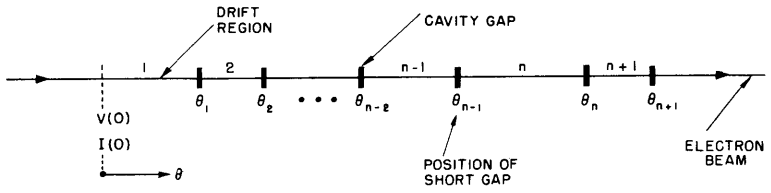

Fig. VI-1. Multicavity klystron.

where $\theta = \beta_q z$ is the plasma transit angle in the direction of electron flow, and $Y_o = \frac{1}{Z_o} = \frac{I_o}{2V_o}\frac{\omega}{\omega_q}$ is the characteristic admittance of the beam.

In a multicavity klystron a drifting electron beam passes through the gaps of the resonant cavities, as shown in Fig. VI-1. If these gaps are very short, the interaction between the gap fields and the electron beam can be formulated (see Fig. VI-2) as follows:

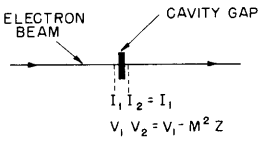

Fig. VI-2. Modulated electron beam passing through a short gap of a cavity.

$$I_2 = I_1 = I \tag{3}$$

$$V_2 = V_1 - M^2 Z I \tag{4}$$

where M is the beam-cavity coupling coefficient and Z is the cavity-gap impedance. If we consider such cavity gaps placed at discrete points along the electron beam, as in Fig. VI-1, then in order to account for the change in kinetic voltage at the gaps, Eq. 1 must be modified according to Eq. 4. The propagation of small signals along the beam of a multicavity klystron with short gaps is then given by

$$\frac{dV}{d\theta} = j Z_o I - \left[\sum_i M_i^2 Z_i u_o(\theta - \theta_i)\right] I \tag{5}$$

$$\frac{dI}{d\theta} = j Y_o V \tag{6}$$

where $u_o(\theta - \theta_i)$ is the unit impulse function that occurs at $\theta = \theta_i$, the position of the i^{th} cavity. The summation extends over all cavities that are of interest. Equations 5 and 6 are analogous to loaded transmission-line equations (3).

Our attention will be focused upon the current modulation in the beam. The kinetic voltage can then be found from Eq. 6. Combining Eqs. 1 and 2, we obtain

$$\frac{d^2I}{d\theta^2} + \left[1 + j\,Y_o \sum_i M_i^2\, Z_i\, u_o(\theta - \theta_i)\right] I = 0 \tag{7}$$

A solution for I can be found as follows. Consider the n^{th} drift region in Fig. VI-1. Equation 7 becomes

$$\frac{d^2I_n}{d\theta^2} + I_n = 0; \qquad \theta_{n-1} < \theta < \theta_n \tag{8}$$

Hence

$$I_n = A_n \cos\theta + B_n \sin\theta \tag{9}$$

Similarly, the current in the (n-1) drift region is

$$I_{n-1} = A_{n-1} \cos\theta + B_{n-1} \sin\theta \tag{10}$$

The boundary conditions at the (n-1) gap are:

(a) The current is continuous

$$I_n = I_{n-1} \text{ at } \theta = \theta_{n-1} \tag{11}$$

(b) The derivative of the current jumps (i.e., the kinetic voltage is discontinuous)

$$\frac{dI_n}{d\theta} = \frac{dI_{n-1}}{d\theta} + j\,Y_o\, M_{n-1}^2\, Z_{n-1}^2\, I \text{ at } \theta = \theta_{n-1} \tag{12}$$

From Eqs. 9, 10, 11, and 12, we obtain

$$A_n = A_{n-1} + j\,Y_o\, M_{n-1}^2\, Z_{n-1}\left(A_{n-1} \sin\theta_{n-1} \cos\theta_{n-1} + B_{n-1} \sin^2\theta_{n-1}\right) \tag{13}$$

$$B_n = B_{n-1} - j\,Y_o\, M_{n-1}^2\, Z_{n-1}\left(B_{n-1} \sin\theta_{n-1} \cos\theta_{n-1} + A_{n-1} \cos^2\theta_{n-1}\right) \tag{14}$$

For any given initial conditions, namely I and V at $\theta = 0$, the current along the successive drift regions is given by Eqs. 9, 13, and 14. An ordinary set of initial conditions is that of a beam excited by an externally driven short-gap cavity. Then, we have

$$\left.\begin{aligned} &I(0) = 0 \\ &V(0) \text{ is finite} \end{aligned}\right\} \tag{15}$$

and hence

$$\left.\begin{aligned} A_1 &= 0 \\ B_1 &= j\, Y_o\, V(0) \end{aligned}\right\} \tag{16}$$

In terms of the slow- and fast-beam waves, the solution to Eq. 8 can be written as

$$I_n = I_n^+ e^{j\theta} + I_n^- e^{-j\theta}; \qquad \theta_{n-1} < \theta < \theta_n \tag{17}$$

Matching boundary conditions at the (n-1) gap, as before, we obtain

$$I_n^+ = I_{n-1}^+ - \frac{1}{2} Y_o\, M_{n-1}^2\, Z_{n-1} \left(I_{n-1}^+ - I_{n-1}^- e^{-j2\theta_{n-1}} \right) \tag{18}$$

$$I_n^- = I_{n-1}^- + \frac{1}{2} Y_o\, M_{n-1}^2\, Z_{n-1} \left(I_{n-1}^- + I_{n-1}^+ e^{j2\theta_{n-1}} \right) \tag{19}$$

For the initial conditions of Eq. 15, we have

$$I_1^+ = -I_1^- = \frac{1}{2} Y_o\, V(0) \tag{20}$$

Equation 7 can be simulated conveniently on an analog computer. This is being done at the present time.

An example of current growth along a seven-cavity klystron is shown in Fig. VI-3. The cavities are spaced along the beam equidistantly 60 plasma degrees apart. They

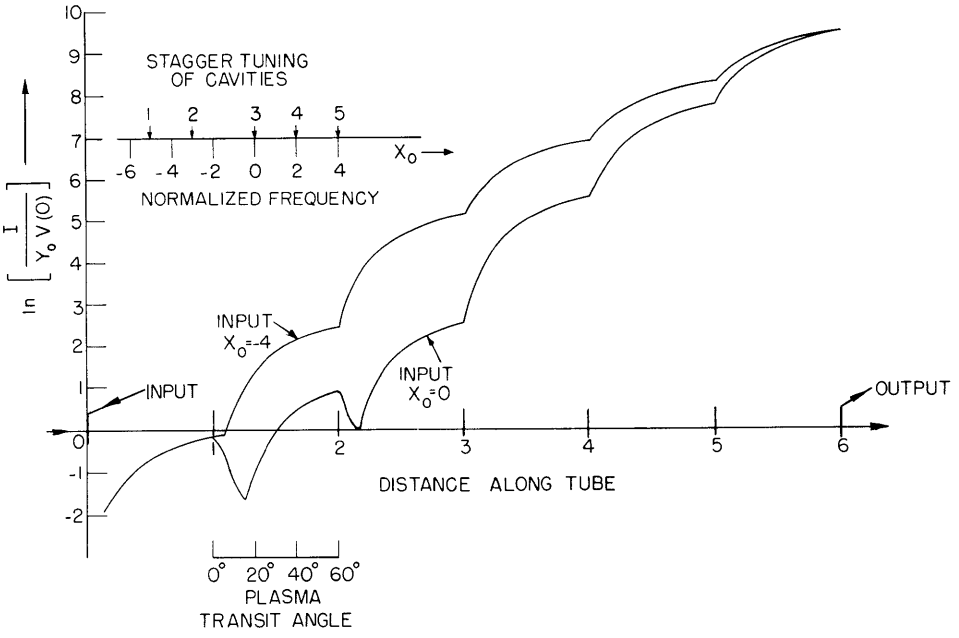

Fig. VI-3. Current growth along a seven-cavity klystron for two input signals of different frequencies.

are assumed to have equal bandwidths (approximately equal Q's); and are stagger-tuned, as shown in the upper left corner of Fig. VI-3. Their detuning with respect to a chosen (normalized) frequency $x_o = 0$ is given in terms of half-bandwidths of the cavities. The input cavity is assumed to be broadband.

The two plots in Fig. VI-3 show current growth along the tube for two frequencies of the input signal. Note that when the current in the beam encounters a capacitive gap (i.e., a gap that is resonant at a lower frequency than the signal), it is debunched, but when it passes through an inductive gap (i.e., a gap resonant at a higher frequency than the signal), it becomes bunched. Maximum bunching occurs in the drift region just after the gap that is resonant at the signal frequency

A. Bers

References

1. S. Bloom and R. W. Peter, Transmission-line analog of a modulated electron beam, RCA Review 15, 95-112 (1954).
2. H. A. Haus, Analysis of signals and noise in longitudinal electron beams, Technical Report 306, Research Laboratory of Electronics, M.I.T., Aug. 18, 1955.
3. T. Wessel-Berg, An analogy between multi-cavity klystrons and loaded transmission lines, Internal Memorandum No. 352, Microwave Laboratory, Stanford University, Dec. 1956.

D. HOLLOW-BEAM KLYSTRON*

The seven-cavity, stagger-tuned, hollow-beam klystron described in the Quarterly Progress Report of April 15, 1957, page 47, is being designed. Most of the work has been concerned with the detailed design of the intermediate and output cavities, and with details of gun fabrication.

The shop is fabricating some stainless-steel prototype cavities.

H. Fock, A. Czarapata

E. NEW METHOD OF MEASURING THE CORRELATION BETWEEN KINETIC-VOLTAGE AND BEAM-CURRENT FLUCTUATIONS

The lower limit of the noise figure (1) of a microwave beam amplifier is given by

$$F_{min} = 1 + \frac{2\pi}{kT}\left(1 - \frac{1}{G}\right)(S\text{-}\Pi) \qquad (1)$$

* This work was supported in part by the Office of Naval Research under Contract Nonr 1841(05).

where T is the temperature of the circuit, G is the available gain of the amplifier, and $S - \Pi$ is the critical noise parameter determined by the noise process near the potential minimum. Although the expression $S - \Pi$ can be considered to be a single noise parameter, it has been split into two parameters, since both S and Π are independently measurable. The value of S has been measured with reasonable accuracy by many researchers (2, 3, 4). But the value of Π, which is directly related to the correlation between the kinetic-voltage and beam-current fluctuations, has not been fully determined, although two different measurements (3, 4) have been made.

A new measuring method, by using a "directional beam coupler," has been proposed (5) and measurements are being made, although the final results have not been obtained.

The electron beam is associated with the two plasma-wave components, fast-wave and slow-wave, in the same way as a conventional electromagnetic wave which has forward-wave and reflected-wave components. If we define A_1 and A_2 as the self-power density spectra (SPDS) of the fluctuations in the fast-wave and slow-wave modes, and A_{12} as the correlation-power density spectrum (CPDS) of the two modes, then S and Π can be written (1) as

$$\left.\begin{aligned} S &= \left\{ (A_1 + A_2)^2 - 4A_{12}\, A_{12}^* \right\}^{1/2} \\ \Pi &= A_1 - A_2 \end{aligned}\right\} \tag{2}$$

The new measuring equipment, a directional beam coupler, can pick up each of the two wave components just as the conventional directional coupler picks up either the forward-wave component or the reflected-wave component. Therefore, we can measure the ratio A_2/A_1. Since we can measure the noise-current standing-wave ratio, ρ, by the usual sliding-cavity technique, the ratio of Π/S can be obtained by the following equation:

$$\frac{\Pi}{S} = \frac{\rho^2 + 1}{2\rho} \frac{1 - (A_2/A_1)}{1 + (A_2/A_1)} \tag{3}$$

Figure VI-4 is a diagram of the measuring equipment. The vacuum chamber, which contains the electron gun for testing, the beam shutter for shot-noise calibration, and two movable cavities, is approximately the same as the chamber that was previously used (3), although many electrical and mechanical design features have been improved. A third cavity, used for calibrating the equipment by a cw signal, has been added. It has a low loaded Q ($Q_L \approx 60$ at 3000 mc). It is located near the electron gun and is provided with a mechanism for detuning. The outputs of both movable cavities, which are one-quarter plasma wavelength apart, are transmitted through the precision attenuators and phase shifters, and, finally, both are added in the Magic Tee. The output of

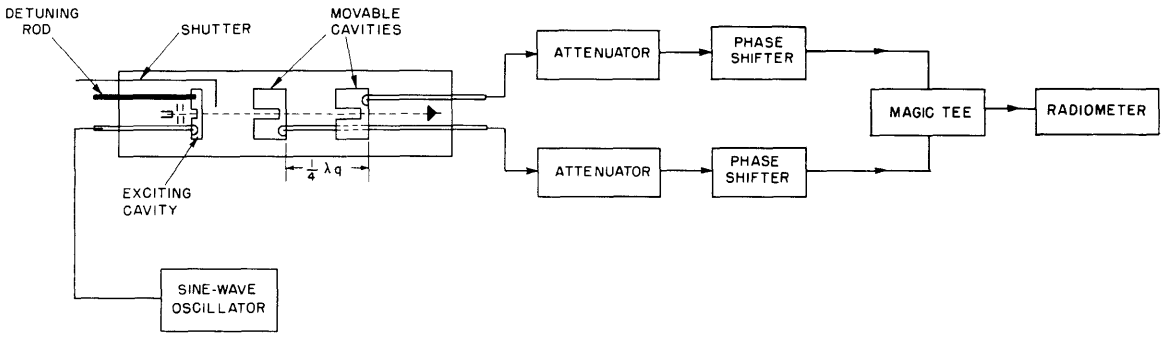

Fig. VI-4. Diagram of measuring equipment.

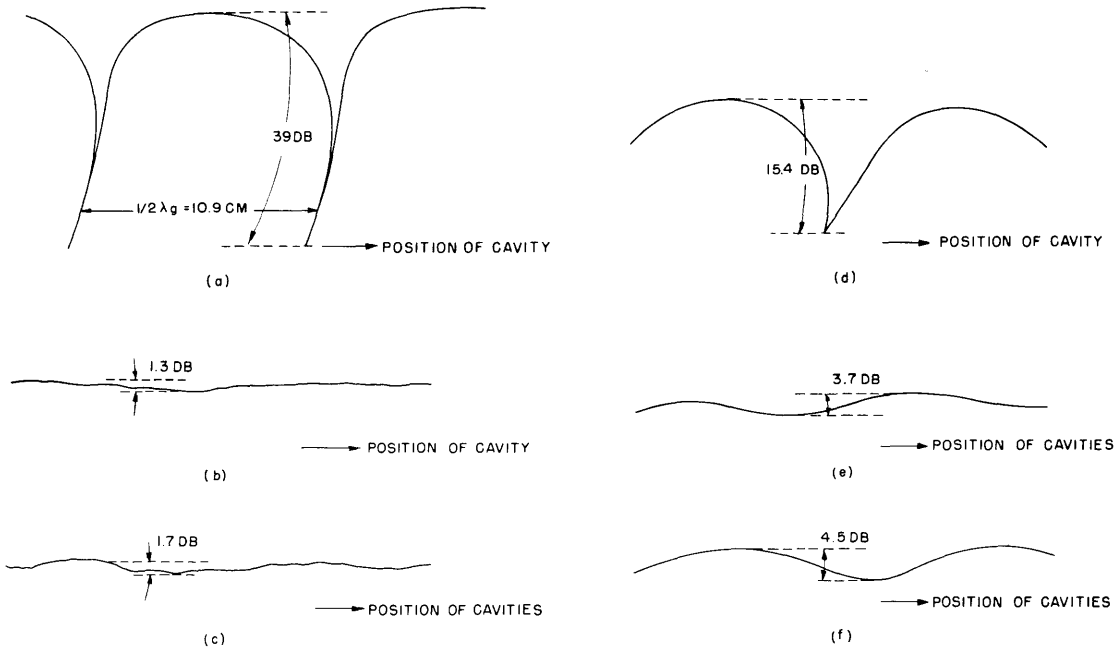

Fig. VI-5. Example of measured results: (a) output of one cavity (sine wave); (b) output of a directional beam coupler I (sine wave); (c) output of directional beam coupler II (sine wave); (d) output of one cavity (noise); (e) output of directional beam coupler I (noise); (f) output of directional beam coupler II (noise).

either the H- or E-branch of the Magic Tee is fed to the radiometer. By proper adjustment of the phase shifters and attenuators, we can get the directional-coupler condition, i.e., the two outputs of the Magic Tee correspond to the fast-wave and slow-wave components. Such an adjustment can be made with the sine-wave signal which is fed into the low-Q exciting cavity (this cavity is detuned in the noise measurement so that it does not effect the beam noise).

One measured example is shown in Fig. VI-5. Figure VI-5a shows the pure standing-wave pattern picked up by only one cavity in the case of sine-wave excitation. In Fig. VI-5b and c the outputs of the directional beam coupler (flat response indicates good directivity of this coupler) are shown. Figure VI-5d, e, and f corresponds to Fig. VI-5a, b, and c in the measurement of beam noise. More measurements will be reported in the next report.

S. Saito, S. Holly

References

1. H. A. Haus and F. N. H. Robinson, The minimum noise figure of the microwave beam amplifier, Proc. IRE 43, 981-991 (1955).
2. W. R. Beam, R. C. Knetchi, and R. W. Peter, Quarterly Reports, Research and development on microwave generators, mixing devices, and amplifiers, David Sarnoff Research Center, RCA Laboratories Division, Princeton, N. J., 1955-1956.
3. A. Bers, S.M. Thesis, Experimental and theoretical aspects of noise in microwave tubes, Department of Electrical Engineering, M.I.T., Aug. 1955.
4. T. J. Connor, Minimum noise figure of traveling-wave amplifiers, S.M. Thesis, Department of Electrical Engineering, M.I.T., Aug. 20, 1956.
5. S. Saito, Beam noise measurement, Quarterly Progress Report, Research Laboratory of Electronics, M.I.T., Jan. 15, 1956, p. 46.

F. BEAM LOADING AT HIGHLY RELATIVISTIC VELOCITIES

Slater (1) has compared the particle energy in standing-wave and traveling-wave linear accelerators with negligible beam loading. Since his analysis, high-current accelerators have become increasingly important. Johnson (2) and others have analyzed the effect of beam loading in traveling-wave accelerators. The effect of beam loading in standing-wave structures is considered here, and compared with traveling-wave structures.

1. Standing-Wave Systems

If we consider a typical standing-wave accelerator cavity, with a gap length between irises of $\lambda/2$, the energy gained by an electron traversing this gap will be

$$\Delta E = \frac{e\mathscr{E}_o}{\beta} \int_{0+\omega t_o}^{\pi+\omega t_o} \sin^2 \omega t d(\omega t) \qquad (1)$$

$$= \frac{e\mathscr{E}_o \lambda}{4} \cos \omega t_o$$

where $\mathscr{E}_o$ is the peak electric field, λ is the free-space wavelength, β is the propagation constant $\left(\beta = \frac{2\pi}{\lambda}\right)$, and t_o is the time of entry of a particle with respect to the zero-field time. The velocity of the particles is assumed to equal the velocity of light. The maximum voltage across the gap can be written in terms of the peak field

$$V_1 = \frac{\mathscr{E}_o \lambda}{\pi} \qquad (2)$$

If we consider a total charge Q uniformly spread from $-t_o$ to $+t_o$, we can integrate Eq. 1 over the interval and obtain the total energy gained by the bunch while it traverses the gap:

$$\Delta E_T = \frac{Q}{\beta 2 t_o c} \int_{-\omega t_o}^{\omega t_o} \frac{\mathscr{E}_o \lambda}{4} \cos \omega t d(\omega t) \qquad (3)$$

Then, if we integrate and average over the time interval, the average power delivered to the beam is obtained.

$$P_b = \frac{I_o V_1 \pi}{4} \frac{\sin \omega t_o}{\omega t_o} \qquad (4)$$

where V_1 is defined in Eq. 2, and $I_o = \frac{Q}{\lambda/c}$ is the average beam current.

In order to maximize this power, V_1 must maximized for a given amount of input power. This can be done by adjusting the coupling to the accelerating cavity. From a lumped-circuit model, we may think of the incident power as a constant-current generator with the internal impedance of the input guide. This would be true only when we are working into a matched load, but if it is assumed that we can adjust the coupling to the source, the approximation is good. With this assumption, the equivalent circuit of the source accelerator structure is given in Fig. VI-6.

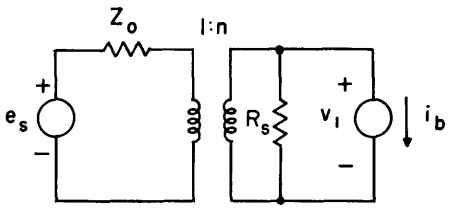

Fig. VI-6. Equivalent circuit of cavity with sources.

If we consider that all quantities are rms, the power flow into the beam is $P_b = V_1 i_b$. Solving for V_1, we obtain

$$P_b = \frac{\frac{e_s}{Z_o n} - i_b}{\frac{1}{Z_o n^2} + \frac{1}{R_s}} i_b \tag{5}$$

P_b can then be maximized for a given source voltage and beam current by adjusting the coupling ratio. Setting $dP_b/dn = 0$, we have

$$n = \frac{-2i_b R_s Z_o \pm \left[(2i_b R_s Z_o)^2 + 4Z_o R_s e_s^2\right]^{1/2}}{2Z_o e_s} \tag{6}$$

which, for large beam loading $\left(i^2 R_s Z_o \gg e_s^2\right)$, becomes

$$h \approx \frac{e_s}{2i_b Z_o} \tag{7}$$

giving a power delivered to the beam of

$$P_b \approx \frac{e_s^2}{4Z_o + \frac{(e_s/i_b)^2}{R_s}} \tag{8}$$

where i_b is found from Eq. 4. We define the efficiency η as the ratio of power delivered to the beam to available power. Thus

$$\eta_{max} = \frac{4Z_o}{4Z_o + \frac{(e_s/i_b)^2}{R_s}} \tag{9}$$

This maximization process also gives the maximum energy gain of an individual particle.

If the bunches are not riding at the maximum accelerating field, the induced back voltage will not be 180° out of phase with the applied voltage. This will introduce a reactive term equivalent to a detuning of the cavity; therefore the cavity tuning will have to be adjusted, as well as the coupling.

A gap smaller than π can be analyzed, but the fringing fields caused by the finite iris hole must then be considered. For an infinitesimal gap with a finite-diameter drift tube, Eq. 4 is multiplied by the factor

$$\frac{4}{\pi}\,\frac{a^2}{a^2+\beta^2} \tag{10}$$

where a is the decay constant in the drift tube.

2. Traveling-Wave Systems

The beam loading in a traveling-wave structure can be determined in a more general manner than is usually done, in order to take into account particles that are not riding on a wave crest. By an analysis similar to that in Section VI-F1, the field of a single traveling wave arising from the beam alone, for a $\lambda/4$ cavity, is

$$\mathscr{E}_{t\omega} = \frac{\lambda}{8}\,\frac{r_s}{\ell_o}\,I_o \tag{11}$$

where r_s is the shunt impedance per meter of the guide, and ℓ_o is the loss length in meters — that is, ℓ_o is the distance in which the power falls to 1/e of its initial value in an unloaded traveling-wave structure. If we now consider n such sections, the forward traveling waves excited in each section will add in phase, while the backward traveling waves will almost cancel. The forward traveling waves can then be added at any point, if we remember that the individual waves decay exponentially because of guide losses.

$$\mathscr{E}_b = \frac{\lambda}{8}\,\frac{r_s}{\ell_o}\,I_o\left(1 + e^{-\lambda/8\ell_o} + e^{-2\lambda/8\ell_o} + \ldots e^{-n\lambda/8\ell_o}\right)$$

$$= \frac{\lambda}{8}\,\frac{r_s}{\ell_o}\,I_o\,\frac{1 - e^{-n\lambda/8\ell_o}}{1 - e^{-\lambda/8\ell_o}} \tag{12}$$

For $\lambda \ll 8\ell_o$, which will always be true, Eq. 12 reduces to

$$\mathscr{E}_b = r_s\,I_o\left(1 - e^{-z/2\ell_o}\right) \tag{13}$$

The discrete variable $n\lambda/4$ has been replaced by a continuous function of distance, z.

The total field at the particle can now be written

$$\mathscr{E}_T = \mathscr{E}_c - \mathscr{E}_b \tag{14}$$

$$\mathscr{E}_c = \mathscr{E}_1 \sin\phi e^{-z/2\ell_o} \tag{15}$$

Equation 15 gives the usual field relation in an unloaded guide.

The energy gained by a particle is

$$E = \int_0^{z_o} \mathscr{E}_T\,dz \tag{16}$$

and the efficiency is

$$\eta = \frac{EI_o}{P} \tag{17}$$

where P is the incident power. Combining Eqs. 13, 14, 15, 16, and 17, we obtain

$$\eta = \left(\frac{r_s}{\ell_o}\right)^{1/2} \frac{I_o}{\sqrt{P}} \left[2\ell_o \sin\phi \left(1 - e^{-z_o/2\ell_o}\right) - m\left\{ z_o - 2\ell_o \left(1 - e^{-z_o/2\ell_o}\right)\right\}\right] \tag{18}$$

where

$$m = \left(\frac{r_s}{P}\ell_o\right)^{1/2} I_o$$

If we maximize η with respect to ℓ_o for a given length of accelerator, we have

$$e^{-z_o/2\ell_o} = \frac{m}{\sin\phi + m} \tag{19}$$

The maximum efficiency of standing-wave and traveling-wave accelerators can now be compared for a given set of input conditions. A comparison was made for a numerical example in which P = 4 Mw, I_o = 0.25 amp, and $r_s = 5.10^7$ ohms/meter. For the sake of simplicity, an infinitesimal bunch traveling on the wave crest was assumed. Efficiency is plotted against accelerator length for the two structures in Fig. VI-7.

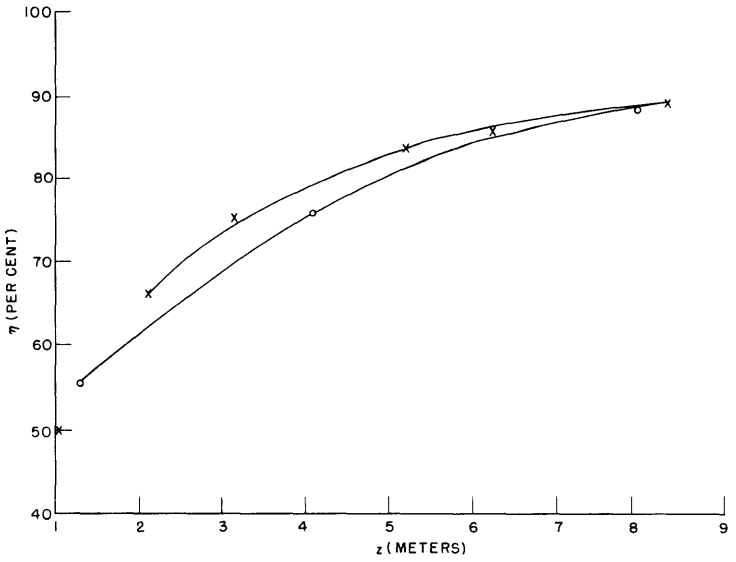

Fig. VI-7. Comparison of efficiency in standing-wave and traveling-wave accelerators.

The efficiencies of standing-wave and traveling-wave accelerators are quite comparable. It must be noted, however, that assignment of identical shunt resistances per meter to the two structures was somewhat unfair to the standing-wave device. Since there are only half as many irises in a π-mode structure as in a $\pi/2$-mode structure, the Q is considerably higher, and the shunt resistance is somewhat higher.

It is possible to decrease the length of a traveling-wave accelerator by means of feedback. In reference 2 this is discussed, and traveling-wave systems with and without feedback are compared. If the particles are not traveling on the crest of the wave, Johnson's formulas must be modified to agree with Eq. 18.

A. J. Lichtenberg

References

1. J. C. Slater, Design of linear accelerators, Revs. Modern Phys. 20, 473 (1948).
2. K. Johnson, On the Theory of the Linear Accelerator (Chr. Michelsens Institutt, Bergen, 1954).